REPORT DOCUMENTATION PAGE

Form Approved
OMB No. 0704-0188

PLEASE DO NOT RETURN YOUR FORM TO THE ABOVE ADDRESS.

1. REPORT DATE *(DD-MM-YYYY)*	2. REPORT TYPE	3. DATES COVERED *(From - To)*
29-12-2020	Final	30 Sept 2016 - 1 Oct 2020

4. TITLE AND SUBTITLE

Bubbling Underwater to Breakup Biofilms and Lift Early Settlers (BUBBLES)

5a. CONTRACT NUMBER

5b. GRANT NUMBER

N00014-16-1-3000

5c. PROGRAM ELEMENT NUMBER

6. AUTHOR(S)

James Bird

5d. PROJECT NUMBER

5e. TASK NUMBER

5f. WORK UNIT NUMBER

7. PERFORMING ORGANIZATION NAME(S) AND ADDRESS(ES)

TRUSTEES OF BOSTON UNIVERSITY
BOSTON MA 02215-1390

8. PERFORMING ORGANIZATION REPORT NUMBER

9. SPONSORING/MONITORING AGENCY NAME(S) AND ADDRESS(ES)

ONR NAVAL MATERIALS DIV
875 N. Randolph Street
Arlington VA 22203-1995

10. SPONSOR/MONITOR'S ACRONYM(S)

11. SPONSOR/MONITOR'S REPORT NUMBER(S)

12. DISTRIBUTION/AVAILABILITY STATEMENT

Approved for public release; distribution unlimited

13. SUPPLEMENTARY NOTES

14. ABSTRACT

This document is the final technical report for ONR grant N00014-16-1-3000. The project investigates the mechanisms by which a stream of underwater bubbles that flow past a surface can prevent biofouling accumulation. Combining high-speed experimental imaging and multiphase numerical simulations, the shear stresses and cleaning efficiency of isolated rising bubbles was deduced. In addition, the dynamics of direct contact of bubble with submerged surface were related to the properties of the surface, bubble, and surrounding liquid. Finally, extending approaches used in integral plume theory and larval settlement, the effects of flowrate on bubble lateral motion and lull periods were related to spatial variation in macrofouling observed in field experiments. The project helped train a postdoctoral researcher, three doctoral students, and two undergraduate students.

15. SUBJECT TERMS

Biofouling, Bubbles, Multiphase Fluid Dynamics

16. SECURITY CLASSIFICATION OF:			17. LIMITATION OF ABSTRACT	18. NUMBER OF PAGES	19a. NAME OF RESPONSIBLE PERSON
a. REPORT	b. ABSTRACT	c. THIS PAGE			JAMES ARMISTEAD
U	U	U	UU	13	19b. TELEPHONE NUMBER *(Include area code)*

Final Technical Report

ONR grant N00014-16-1-3000

BUBBLES: Bubbling Underwater to Breakup Biofilms and Lift Early Settlers

1. Executive Summary

This is a final technical report for ONR grant N00014-16-1-3000 entitled "BUBBLES: Bubbling Underwater to Breakup Biofilms and Lift Early Settlers". The goal of this grant was to better understand the fluid mechanics associated with aeration grooming, a strategy that reduces the buildup of biofouling organisms by passing a continuous stream of air bubbles over the submerged surface. In particular, the grant explored grooming from isolated rising bubbles, the dynamics that occur when a bubble direct contacts a submerged surface, and the effects of flowrate on the lateral motion of bubble stream. The technical approach used to investigate these phenomena included multiphase numerical simulations, high-speed experimental imaging, and the development of physical models and scaling laws. The project helped in the training of a postdoctoral researcher, three doctoral students, and two undergraduate students.

The studies related to grooming from isolated rising bubbles combined numerical simulations and simulations to estimate the shear stress from a bubble rising along an inclined wall. As part of this research, we found that bubbles can remove adhered fouling over a range of inclination angles. At low inclination angles, the bubbles slide on the surface and apply a lower steady cleaning stress; whereas, at high inclination angles, the bubbles bounce and provide a higher spatially varying stress on the wall. Simulation results were consistent with experiments, finding that cleaning can be quantified by the maximum wall stress experienced at each point.

Additional studies investigated the conditions required for bubbles to stick to a surface rather than bounce or slide off. We found that millimeter-sized air bubbles will bounce or slide off of smooth inclined surfaces in water, but will often stick if the surface is superhydrophobic. A similar sticking behavior was observed on liquid-infused surfaces. Furthermore, we discovered that spreading dynamics of a bubble on a liquid-infused surface is predominantly set by inertial and capillary forces, yet depends on the viscosity of the infused immiscible fluid. A combination of experiments and modeling suggests that the bubble transition from bouncing to sticking depends on the mobility of the interface, which can be measured from the rate of spreading of a contacted bubble.

Finally, a combination of experiment and analytical modeling was used to investigate the effects of flowrate on bubble lateral motion and grooming region. We observed that bubbles spread laterally to form a wedge with a shape that depends on flowrate and inclination angle. We discovered that the distribution of bubbles could be accurately modeled using a 2D integral plume theory. Furthermore, we find that a bubble stream provides a unique tool to study fouling in fluctuating liquid environment. In particular, we observe that a bubble stream produces regions with different distributions of lull windows, and we find that locations where the water velocity drops below a few centimeters per second for 0.1 seconds is predictive of macrofouling.

2. Naval Relevance & Impact

Marine biofouling on Navy platforms is problematic, as it can reduce the speed and performance of ships, increases the amount – and therefore cost – of fuel required, and can lead to delays if ships need to be cleaned or quarantined to prevent invasive fouling species from entering a port. Aeration grooming is one approach that may help reduce biofouling growth on parts of a ship while it is pier-side and is advantageous in that it is both environmentally friendly and gentle enough to avoid damaging existing coatings. Understanding bubble-surface interactions can help to determine the cost and feasibility of aeration. Additionally, measurements of the rate of fouling around a bubble streams could provide new insight into the settling dynamics of fouling species and provide a dynamic test to various antifouling surfaces.

3. Publications and Presentations Acknowledging ONR Contract

Oratis, A. T., Bush, J. W., Stone, H. A., & Bird, J.C. (2020). A new wrinkle on liquid sheets: Turning the mechanism of viscous bubble collapse upside down. *Science*, 369(6504), 685-688.

Bird J.C., Menesses M., Brasz C.F., Belden J. "Shaping stress fields with spreading bubble streams: applications for biofouling prevention" Presented at 72nd Annual Meeting, American Physical Society, DFD, Seattle, WA. Nov. 2019.

Dubitsky, L., Menesses, M., Belden J. & Bird, J.C. "Examining the effects of hydrodynamic features on biofouling growth and suppression" Presented at 72nd Annual Meeting, American Physical Society, DFD, Seattle, WA. Nov. 2019.

Brasz, F., Kim, D., Menesses, M., Belden, J. & Bird, J.C. "Bubble plumes beneath an inclined wall" Presented at 71st Annual Meeting, American Physical Society, DFD, Atlanta, GA. Nov. 2018.

Menesses, M., Belden, J., Dickenson, N., & Bird, J.C. "Aeration can prevent biofouling growth provided wall shear stresses exceed a threshold value." Presented at the 19th International Congress On Marine Corrosion And Fouling, Melborne, FL. June 2018.

Belden, J., Menesses, M., Dickenson, N., & Bird, J.C. "Air bubbles induce a critical continuous stress to prevent marine biofouling accumulation." Presented at 70th Annual Meeting, American Physical Society, DFD, Denver, CO. Nov. 2017.

Bird, J.C., Brasz, F., Kim, D., Menesses, M., & Belden, J. "Bubble streams rising beneath an inclined surface." Presented at 70th Annual Meeting, American Physical Society, DFD, Denver, CO. Nov. 2017.

Menesses, Belden, Dickenson & Bird "Measuring a critical stress for continuous prevention of marine biofouling accumulation" *Biofouling* 2017

Several more papers are in various stages of preparation.

4. Technical Discussion of Key Results

4.1. Grooming from isolated rising bubbles

When bubbles impact an inclined surface, they can contact the surface for a short enough time that they slide or bounce off of a thin lubricating liquid film. One key accomplishments from this grant was that we were able to reproduce this motion with numerical simulation that solved the 3D Navier-Stokes equations using the volume-of-fluid technique. Figure 1 illustrates a superposition of the bubble trajectory in experiments along with interface of the bubble from simulations. The simultations are able to replicate the transition from a sliding behavior at shallower inclination angles to bouncing at steeper incliation angles. Past simulations had modeled the trajectory of the bubble but did not simultanteously simulate the shape of the bubble and the flow field of the surrounding liquid. With the flow-field of the liquid, we are able to compute the wall stress as the bubble passes.

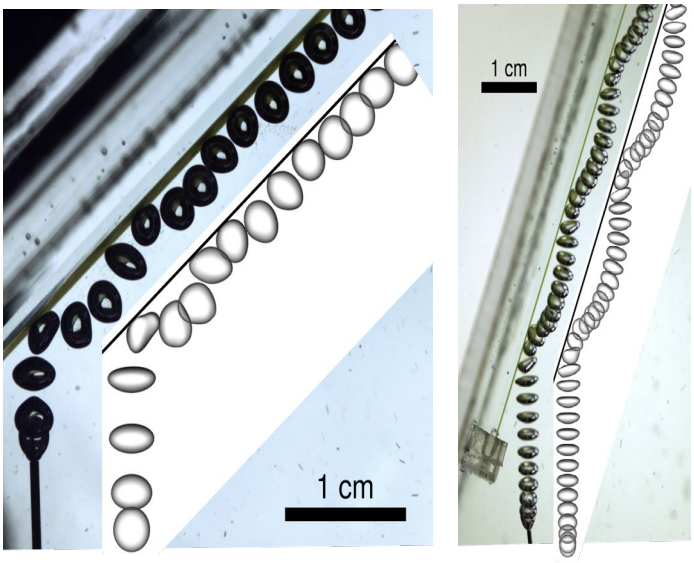

Figure 1. Our numerical simulations of a single bubble rising against an inclined wall can capture a bouncing to sliding transition between different inclination angles that we also observe with high-speed optical visualization experiments.

We hypothesized that the the scubbing potential of a bubble could be quantified by the wall stress and that this stress would depend on inclination angle. However whether a steeper or shallower inclination angle would lead to higher stress was not clear. Specifically, at a lower angle, bouyant forces would draw the bubble closer to the surface than at a higher inclination angle; yet the tangential bubble speed would be slower. Complicating these dynamics are the shift from sliding to bouncing behavior.

The wall stress at each point on the wall varies with time as the bubble passes by. Vorticity generated in the liquid continues to apply a stress on the wall well after the bubble has left that region. We speculate that the removal of a fouling organism would depend on the maximum wall stress that it experienced. Thus from the numerical simulations, we calculate the maximum wall stress experienced at each point on the wall as a bubble passes (Fig. 2A). Note that there are locations on the wall where the stress from the bubble exceeds 40 Pa, yet only a small fraction of the area the bubble traverses experiences this level of elevated stress. A significantly larger area of wall experiences stresses between 15 and 20 Pa. As expected, there are noticible differences in the spatial variation in wall stress for bubbles that bounce and bubbles that slide. Interestingly, when a bubble bounces on the surface, the largest stresses surround the footprint rather than occuring in its middle. The

liquid velocity leading to this stress is also typicaly downward, rather than moving upward with the bubble.

In collaboration with Prof. Aizenberg's group at Harvard University, we were able to grow algae on the surface of the glass slides, incline them at various angles, and investigate what remains after 25 bubbles have passed over the surface. The difference in algae cover is illustrated in Figure 2A along with the corresponding stress maps from the numerical simulations. The spatial variation in algae removal clearly correlates with the spatial values off the maximum wall stress, indicating that this metric is appropriate to quantify removal. Furthermore, the removal footprints that correspond to a bubble bounce have the higher removal around where a bubble bounces than in the middle, following the same pattern as the maximum shear stress (Fig. 2A).

Finally, we can use these results to calculate a cleaning efficiency. Here, we define the cleaning efficiency as the fraction of locations in which shear stress exceeds a critical value – such as the value needed to dislodge a fouling organism – relative to the area that bubble passes

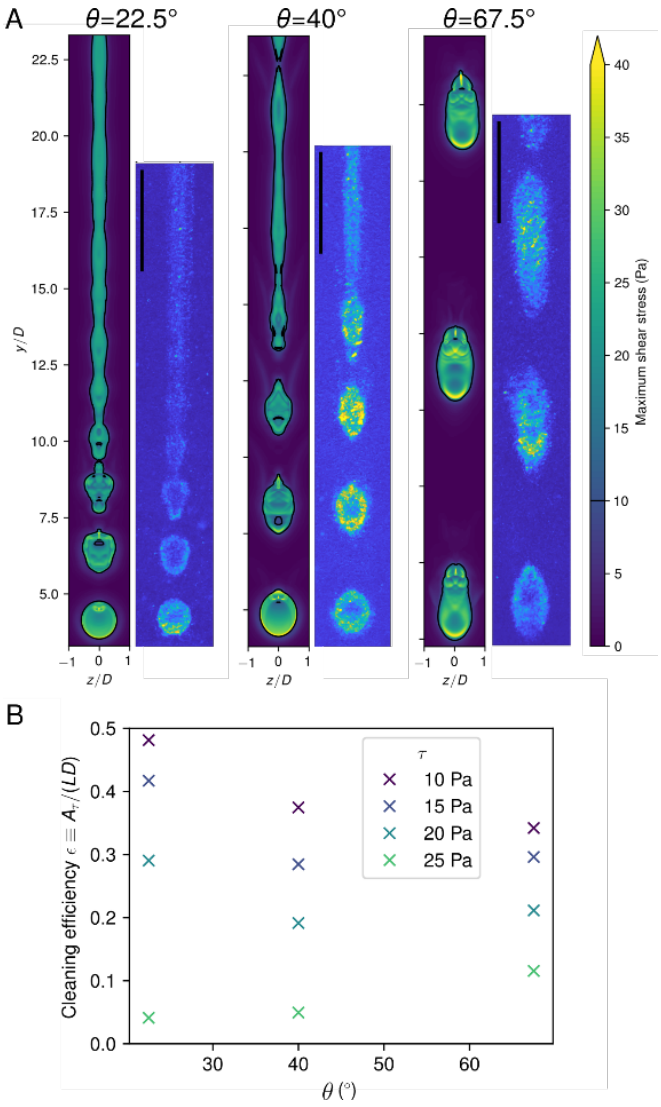

Figure 2. (A) The shear stress at the surface is calculated during a bubble pass from the numerical simulations and shows a similar spatial pattern to the removed algae. This pattern changes with varying inclination angle as the bubbles switch from predominantly sliding to bouncing. **(B)** If we define a cleaning efficiency as the amount of area that is cleaned relative to the area of the strip that the bubble passes, we find that the efficiency depends on both the angle and the shear stress required to dislodge the fouling organism. For less-adhered organisms, a lower angle will lead to a higher efficiency; whereas at more-adhered organisms, a higher angle will lead to higher efficiency. This response can be attributed to the time that the bubble passes at various distances from the surface.

(Fig. 2B). Unsurprisingly, the cleaning efficiency increases as the critical stress is lowered. We find that at high inclination angle, the bubble is more efficient at removing highly adhered material than at a lower inclination angle. However, we also find that at a lower inclination angle, the bubble is more efficient at removing marginally adhered material than at a higher inclination angle. For critical shear stresses below 20 Pa, sliding is more efficient at cleaning than bouncing due to the area that is missed while the bubble separates from the surface during the bounce. However, when the critical shear stress is above 20 Pa, bouncing is more efficient due to the larger stress that develops as the bubble impacts and rebounds from the surface. Separate microfluidic experiments with the algae, suggest that removal begins when the shear stress exceeds 9 Pa, and indeed removal is consistent with computations for shear stress at this level. Taken together, the results highlight that bubbles can remove (rather than just prevent) adhered fouling at a variety of inclination angles, and support that this cleaning can be quantified by the maximum wall stress experienced by the surface.

4.2. Dynamics of direct contact of bubble with submerged surface

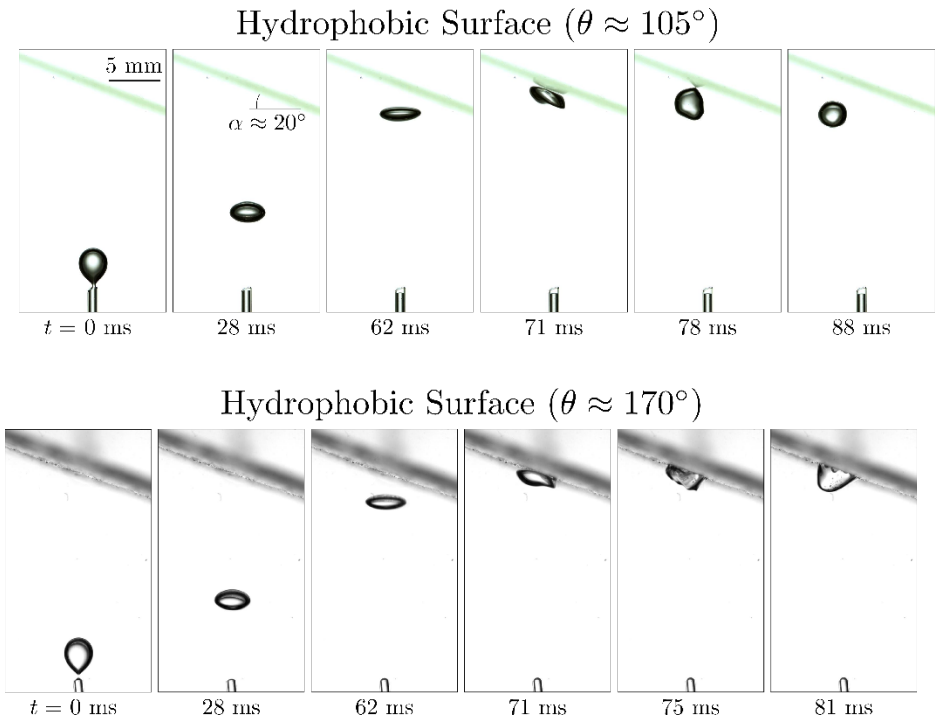

Figure 3. We are also interested in understanding the conditions that would cause bubbles to contact and stick to an underwater surface rather than bounce or slide along it. (Top) High speed camera images of an air bubble as it rises in water and bounces off of a surface with similar hydrophobic contact angle to commercial foul-release coatings. (Bottom) Under the same conditions, the bubble would stick to the surface if it were superhydrophobic and had a thin air layer trapped within a microstructure.

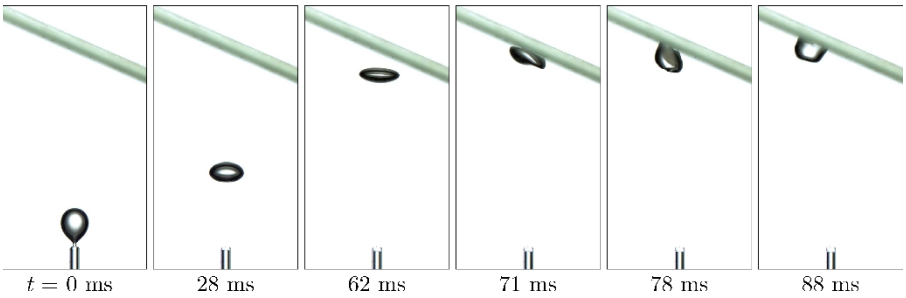

Figure 4. We have found that contact angle alone is not the sole surface property that determines whether or not a bubble will stick or bounce. Under the same bubble impact conditions as in Fig. 3, the bubble will stick to the oil-infused microtextured surface, even though the contact angle is similar to that in the top images of Fig. 3.

When a bubble slides or bounces on a surface, there is a thin liquid film that separates the air in the bubble from the solid. If this film ruptures, it can rapidly dewet, and the bubble can directly contact and stick to the submerged surface. As part of the research in this grant, we carried out experiments to investigate the conditions required for bubbles to stick to a surface rather than bounce or slide off. We found that in almost every instance, millimeter-sized air bubbles will bounce or slide off of smooth inclined surfaces in water, even if those surfaces are hydrophobic (Fig. 3, top). Interestingly, we find that if the surface is superhydrophobic (microtextured and hydrophobic), a bubble is more apt to coalescence with the surface, even at fairly steep angles (Fig. 3, bottom). This result highlights the importance of dynamic wetting in this process and by extension the role of the equilibrium contact angle. Perhaps most surprisingly, we find that bubbles can stick to oil-infused surfaces in cases in which they would bounce on a surface with an equivalent contact angle (Fig. 4). This finding indicates the importance of surface characteristics beyond the contact angle and opens the possibility that different interfacial dynamics are important on a rigid smooth surface as opposed to one with microscopic roughness containing trapped immiscible liquid or gas.

To probe the properties of the interface on the dewetting dynamics, we gently deposit a bubble onto a horizontal submerged solid and record the spontaneous spreading with high-speed optical visualization. We modify glass slides with different silanes to vary the contact angles. In addition, we use a commercial nanotexured surface coating that either is used to make a glass slide superhydrophobic or – in the presence of a drop of silicone oil – liquid infused. Figure 5 illustrates the spreading distance as a function of time for the different surfaces. The spreading follows a power-law dynamic, which is revealed using a log-log graph. For the superhydrophobic surface, the bubble spreads at the same speed as it would if it were to coalesce with the free surface. Specifically, the spreading of the bubble is equivalent to the rapid dewetting of a thin axisymmetric film with parabolic thickness variation driven by surface tension and regulated by the inertia of the film. As such, the spreading depends on the bubble size, surface tension, and liquid density in a way that can be normalized to a set of universal curves when plotted with the dimensionless parameters on the axes of Fig. 5.

Interestingly, the spreading dynamics on solid smooth surfaces are about an order of magnitude slower than on the superhydrophobic surface. The particular smooth surface in

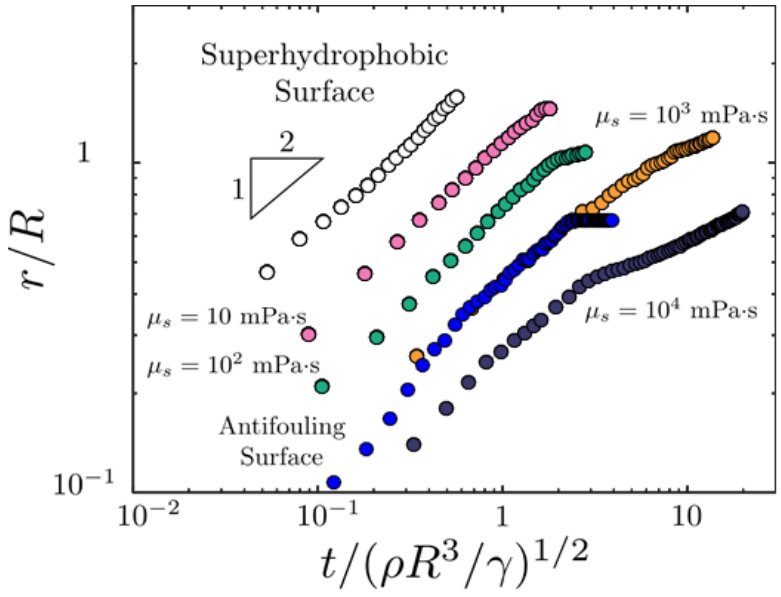

Figure 5. Measurements of how a bubble spontaneously spreads upon contacting a surface plotted on a log-log graph. The spreading radius r is normalized by the initial bubble radius R, and time t is non-dimensionalized by an inertial-capillary timescale that depends on density ρ and surface tension γ. We find the rate of spreading is faster for the superhydrophobic surface than the antifouling surface. We also find that liquid-infused surfaces can vary depending on the viscosity of the infused oil.

Figure 5 is the foul-release coating, Intersleek 900. The liquid infused surfaces spread at speeds that vary with the viscosity of the infused silicone oil. Yet, our experiments found that the spreading dynamics stopped varying with this viscosity at sufficiently low and high viscosity and followed an inertial scaling in these limits. Collectively these results suggest that the transition from bouncing to sticking depends on the mobility of the interface, which can be measured from the rate of spreading of a contacted bubble.

For spreading on smooth solid surfaces, we found that the power law dynamics shift to a higher power at early times that is closer to $r \sim t^{2/3}$ than $r \sim t^{1/2}$. Previous models differed on the underlying physics responsible for the spontaneous spreading dynamics. Specifically, it is unknown whether the dynamics are regulated by inertia or viscosity in the presence of a moving contact line. Our experimental results demonstrated that neither the inertial or viscous model is appropriate in this regime. We developed a new conceptual model in which inertia and viscosity are coupled with the moving contact line of the retracting liquid film. This model can account for the shift in the power law dynamics and has the potential to provide macroscopic insight into microscopic contact line dynamics.

Another outcome of this grant has been new understanding on the dynamics of curved, viscous fluid films. The drainage and rupture of thin liquid films occur when bubbles approach and contact a surface. They also are relevant in a variety of coating processes, such as when applying spray paint. It has been known that curved viscous films can wrinkle, with the phenomenon attributed to gravity. We have shown that surface tension, not gravity is responsible for this effect and have demonstrated how surface tension can initiate dynamic buckling. These findings suggest that these film dynamics are independent of orientation and may be at scales that could be important for certain coatings.

4.3. Effects of flowrate on bubble lateral motion and grooming region

In addition to considering single rising bubbles, this grant considers streams of bubbles that rise one after another from the same location. At moderate flowrates, we observed that the trajectories of bubbles spread laterally to form a wedge shape in aggregate as they rose. This pattern is similar to the wedge-shape clean regions observed in our field data. To systematically investigate this effect, we recorded 10,000 frames of air bubbles rising for 4 different inclination angles and 11 different flowrates. By superimposing these images, we can see how these parameters effect the lateral migration of bubbles along the surface (Fig. 6). From these images we can calculate the probability that a bubble will be passing a particular location, which is equivalent to the average void fraction distribution *f(x,y)*. From this distribution, we can calculate a wedge profile for which most bubbles are contained (dotted lines in Fig. 6). By tracking the centroids of the bubbles, we can also calculate the average bubble rise velocity (background color in Fig. 6), which we find does not vary significantly as the bubbles rise.

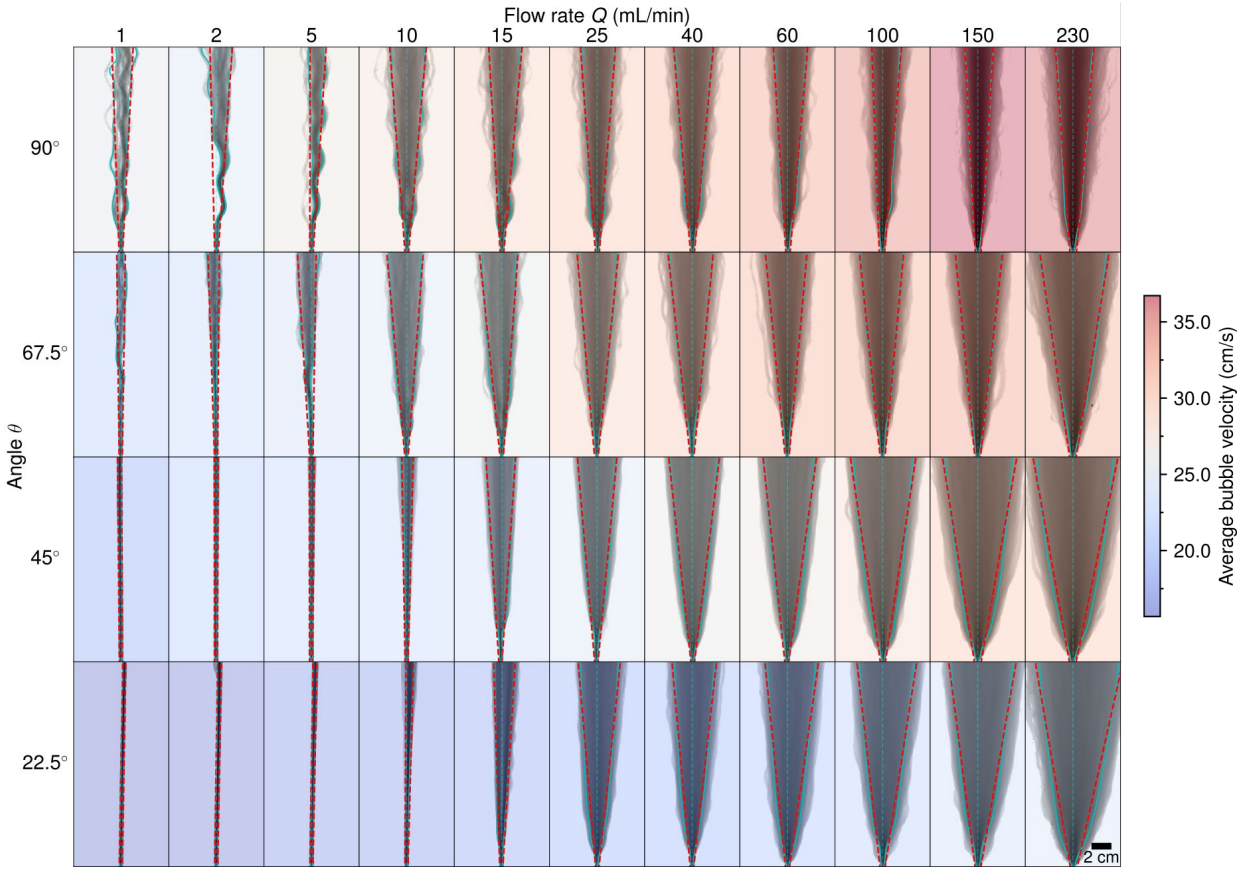

Figure 6. Cumulative position of bubbles on surface for various flow rates and inclination angles. Collectively, the bubbles disperse laterally as they rise, sweeping out a wedge pattern. The color of overlaid on each tile represents the average velocity of bubbles once they reach 5 cm above the nozzle.

As part of this grant, we have developed a theoretical grounding for our experimental results on meandering of bubble streams by extending ideas from integral bubble plume theory. The central idea is that rather than investigate the individual trajectories and interactions between bubbles, we can take a statistical approach and model the *average* velocity u and void fraction f at each point (x,y) on the surface. We assume that at each height y, the average velocity and void fraction can be modeled with Gaussian distributions in terms of the horizontal distance from the centerline x (Fig. 7). The width of the liquid velocity distribution $b(y)$ depends on height y and the width of the void fraction distribution is assumed to follow the same relative function, but with a scaling factor λ. Finally, we assume that the bubbles are confined to a thickness h that is approximately the bubble diameter (Fig. 7).

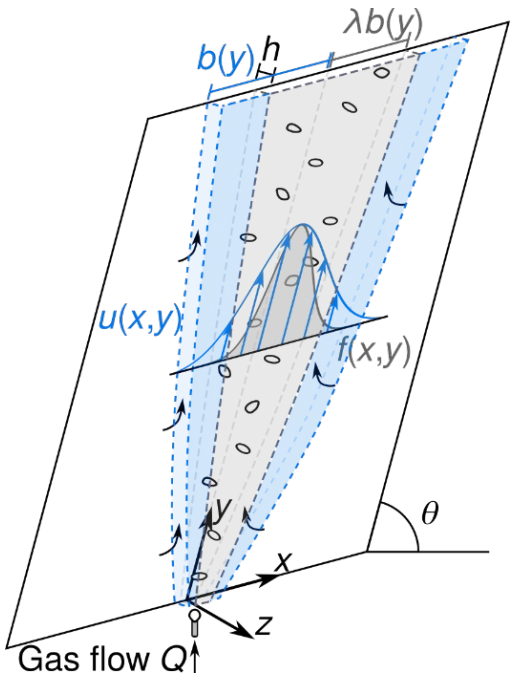

Figure 7. The schematic above shows how bubbles rising from a nozzle will cause the surrounding water to flow at velocity $u(x,y)$, which then causes the bubble distribution $f(x,y)$ to spread outward as the bubbles rise.

Integral equations can be written for conversation of mass of the liquid, conservation of mass of the gas, conservation of momentum, and conservation of energy, which due to Gaussian distributions, can be reduced to a system of ordinary differential equations. By neglecting viscous losses and approximating the centerline velocity as constant, we find analytical solutions to these equations. These solutions predict a wedge shape. Indeed, our analysis suggests that as the flowrate is increased, there is an excess in buoyant potential energy, which translates the particles laterally and increases the rate at which the wedge widens.

We find that our experimental results are consistent with the assumptions and predictions of the model. For example, our model assumes that the average bubble void fraction follows a Gaussian distribution along each horizontal slice. Figure 8 illustrates that void fraction measurements indeed follow the functional form $f(x,y) = F(y)\exp(-x^2/b_g^2(y))$. Along horizontal slices with a constant value of y, the void fraction follows Gaussian distributions with their peak over the bubble center-line (Fig 8b). Furthermore, the experimental results are consistent with predictions that the standard deviation $b_g(y)$ increases linearly with distance from the nozzle y. For each position y, we can identify the location of two standard deviations from the centerline $2b_g(y)$ (cyan curves in Fig. 8a). Note that 98% of the rising bubbles are expected to be contained within these bounds. To highlight that $b_g(y)$ can be approximated as a wedge, best-fit lines are also plotted (red dashed lines in Fig. 8a). The wedge shape is predicted from our 2D plume model and supported by the observations that these two sets of curves (red and cyan curves in Fig. 8a) are nearly indistinguishable.

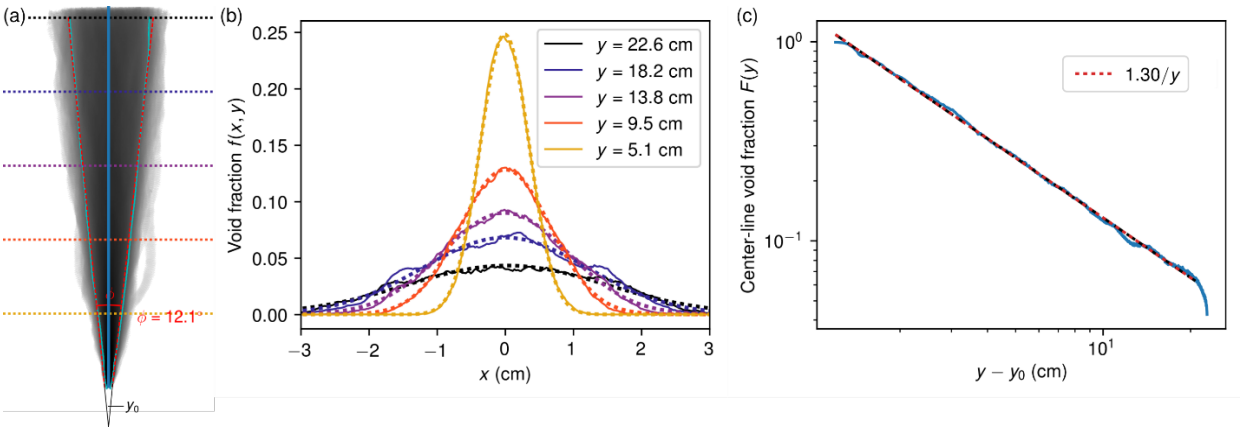

Figure 8. Experimental data confirms model assumptions and predictions for void fraction. (a) A representative void fraction distribution when $\theta = 67.5$ degrees and $Q = 150$ mL/min has a width that extends linearly with height y. (b) The void fractions corresponding to the horizontal slices in part a (colored solid lines) follow Gaussian distributions (colored dashed lines). (c) The center-line void fraction $F(y)$, obtained from the Gaussian fits at each height y, is inversely proportional to y, as predicted by our model. Here y_0 is the offset to account for the finite size of the plume at the bubble nozzle, as illustrated at the bottom of panel a.

A final prediction that our model makes for the bubble void fraction is that as the bubbles disperse laterally, the center-line concentration F(y) is inversely proportional with the distance y. Note that the width of the plume is non-zero at the nozzle ($y = 0$) and the linear fit can be used to identify an appropriate vertical offset y_0 (Fig. 8a). Indeed, plotting the center-line void fraction from the experiments as a function of this vertical distance on a log-log plot, confirms this prediction (Fig. 8c). Collectively these findings support a use of an integral 2D plume model to predict the lateral extent of streams of bubbles on a submerged incline surface. These results allow us to model the spatial variations in bubble concentrations and velocity fields from these bubbles to better understand the mechanisms by which bubbles can prevent and remove biofouling growth.

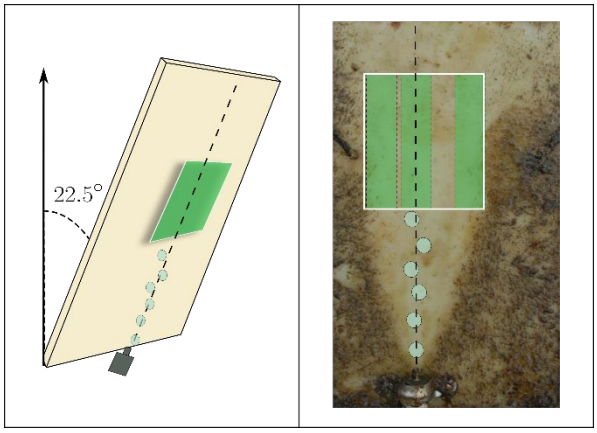

Figure 9. The same bubble flow can be put out in the field and in the lab. In the lab, a laser sheet is use to map out the velocity of the water surround the bubbles using Particle Image Velocimetry (PIV). We correlate the flow structure to the fouling intensity between different regions relative to bubble stream centerline.

To directly relate how the structure of the flow past a surface influences the fouling growth, we revisited our fouling data collected at Narraganset Bay, RI when we passed bubbles streams during the summer over the surface at various bubble flowrates.

frequencies. Instead of considering macrofouling as a binary and examining its spatial extent, we calculate a fouling 'score' that we can correlate with the flow conditions. These fouling scores were collected on panels above the bubble stream along the centerline and at two distances from the centerline, as illustrated in Figure 9. We also replicated the setup in the lab and measured the flow fields tangential to the surface at these locations at a distance from the wall comparable to the radius of the bubbles.

Rather than just considering the average velocity associated with the bubbles or surrounding liquid – or the average shear stresses that they produce – we also consider the temporal variation in these flow fields. Specifically, we can extend the idea of lull windows that are used to predict regions of larval settlement. Various marine larvae generally require the local flow to go below a critical velocity for a fraction of a second in order to attach to the surface. As part of the research for this grant, we have extended these ideas from a single organism quickly settling in the lab to multiple organisms developing a macrofouled community in the field over months.

The approach that we have taken to map out the occurrence of lull windows on the submerged surface is illustrated in Figure 10. At a particular location, PIV flow measurements provide the velocity as a function of time. We can specify two parameters, a critical velocity V_{cr} and a critical time T_{cr}. A lull period occurs whenever the flow velocity drops below the critical velocity; however, it is only when the lull time lasts longer than the critical time that we denote

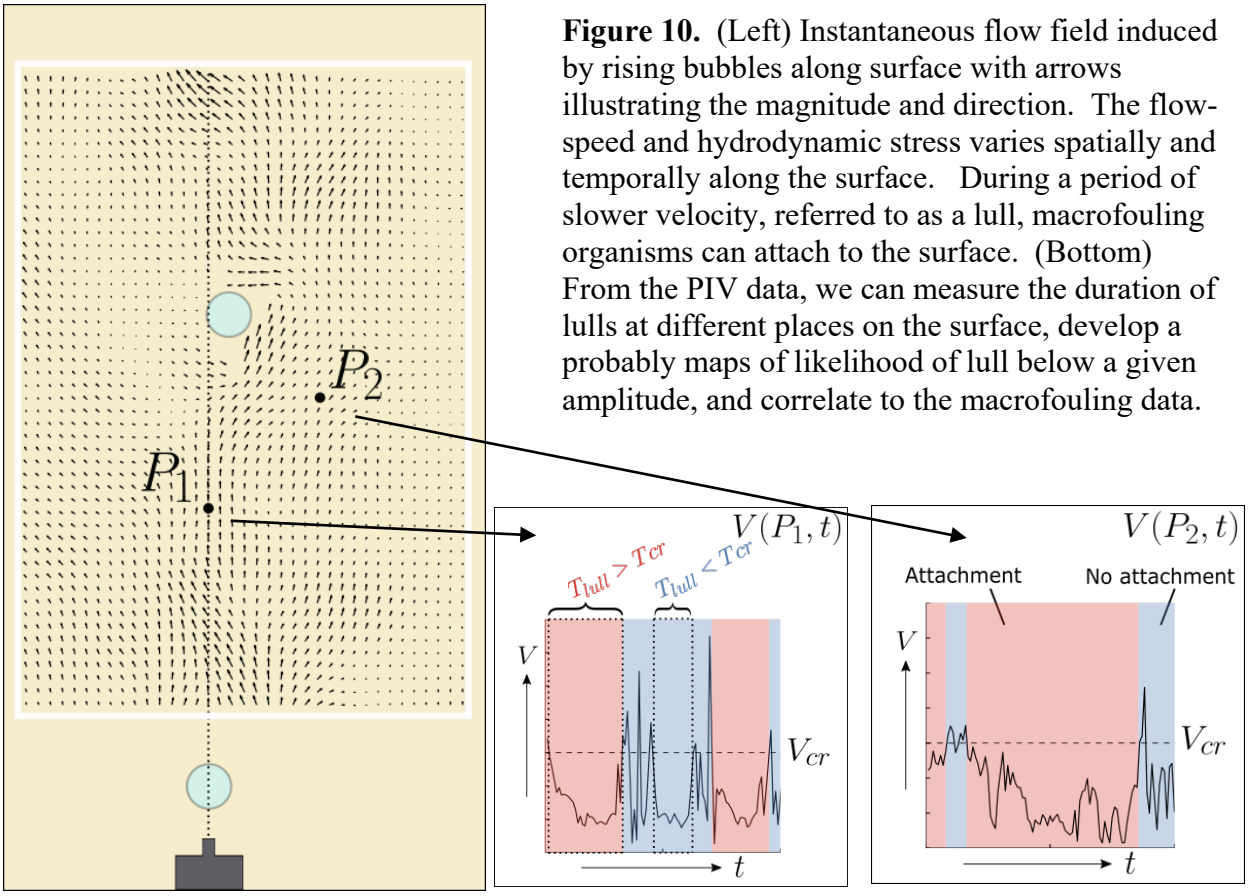

Figure 10. (Left) Instantaneous flow field induced by rising bubbles along surface with arrows illustrating the magnitude and direction. The flow-speed and hydrodynamic stress varies spatially and temporally along the surface. During a period of slower velocity, referred to as a lull, macrofouling organisms can attach to the surface. (Bottom) From the PIV data, we can measure the duration of lulls at different places on the surface, develop a probably maps of likelihood of lull below a given amplitude, and correlate to the macrofouling data.

this time as a potential attachment period (red regions in Fig. 10). The fraction of attachment periods over the entire time window provides a probability that the organism would contact the location during an attachment period.

A bubble stream provides a unique tool to spatially vary the attachment times. Specifically, if bubbles were to follow their centerline and not stray laterally – as occurs for significantly low bubble flowrates – then decreasing the flowrate increases the time between subsequent bubbles and increases the probability of attachment. Similarly, at high enough flowrates where bubbles interact and develop widening plumes, the void fraction decreases laterally, leading to larger probabilities of attachment, even though each bubble rises at roughly the same speed.

By using the fouling scores to tune the critical velocity V_{cr} and a critical time T_{cr}, we can find values of these parameters that best correlate location-specific fouling and attachment probability. We found the presence of lull windows, where the water velocity drops below a few centimeters per second for 0.1 seconds, is predictive of macrofouling. Given that this correlation is fairly strong and better than other predictive metrics, we believe the approach can be used to predict regions of macrofouling in flow, even when bubbles are not present. Interestingly, similar frequency and amplitude lull windows have been previously associated with increased larval settlement, suggesting that it may be more appropriate to view aeration as a proactive cleaning tool that prevents macrofouling settlement than one that grooms and removes established growth.

5. Acknowledgements.

The grant financially supported members of our research team at Boston University who carried out the work outlined in this report. In particular, our team included a postdoctoral researcher (Dr. Frederik Brasz), three graduate students (Lena Dubitsky, Mark Menesses and Alex Oratis), and two undergraduate students (Dianne Kim and Alex Moreno). We also acknowledge contributions to the algae experiments by Stefan Kolle and Cathy Zhang from Prof. Joanna Aizenberg's group at Harvard University. The Intersleek 900 coated samples were provided by Prof. Kelli Hunsucker and Prof. Geoffrey Swain from Florida Institute of Technology. Finally, we acknowledge the intellectual and technical support from the YIP Advisory Board Members: Dr. Jesse Belden and Dr. Natasha Dickenson (NUWC Newport) and Dr. Eric Holm (NSWC Carderock).